The Astrophysical Journal, 584:418–426, 2003 February 10

UNDERSTANDING THE RADIO EMISSION GEOMETRY OF MULTIPLE-COMPONENT RADIO PULSARS FROM RETARDATION AND ABERRATION EFFECTS

Y. Gupta[1]
National Astronomy and Ionosphere Center, Arecibo Observatory, HC3 Box 53995, Arecibo, PR 00612; ygupta@ncra.tifr.res.in

and

R. T. Gangadhara
Indian Institute of Astrophysics, Bangalore 560034, India; ganga@iiap.ernet.in
Received 2002 June 11; accepted 2002 October 21

ABSTRACT

We have conducted a detailed analysis of the emission geometry of a handful of radio pulsars that have prominent, multiple-component profiles at meter wavelengths. From careful determination of the total number of emission components and their locations in pulse longitude, we find that all of the six pulsars show clear evidence for retardation and aberration effects in the conal emission beams. Using this information, coupled with a dipolar field geometry, we obtain estimates of the height and transverse location in the magnetosphere for each of the emitting cones in these pulsars. These results support our earlier conclusions for PSR B0329+54 in that we find successive outer cones (in cases of multiple-cone pulsars) being emitted at higher altitudes in the magnetosphere. The range of inferred heights is from ~200 to 2200 km. The set of "active" field lines from which the conal emissions originate are located in the region from ~0.22 to ~0.74 times the polar cap radius. At the neutron star surface, these conal rings map to radii of a few to several tens of meters, and the separation between successive rings is about 10–20 m. We discuss the implications of these findings for the understanding of the pulsar emission geometry and for current theories and models of the emission mechanism.

Subject headings: pulsars: general — radiation mechanisms: nonthermal — stars: magnetic fields — stars: neutron

1. INTRODUCTION

Radio emission from a pulsar is believed to originate in the open field line region of the polar cap of the neutron star. The size, shape, and location of regions of radio emission in the average profiles of pulsars is thus expected to reflect the arrangement of emission regions in the pulsar magnetosphere. Pulsar average profiles exhibit a great diversity in shape, and their classification based on the number of emission components is a useful starting point to study the emission characteristics of pulsars. Rankin (1990, 1993 and references therein) has carried out such a detailed classification and has come to the conclusion that there are two kinds of emission components—core and conal—in pulsar profiles, which result from two distinct types of emission mechanisms. Further, Rankin proposes that the conal components arise from two nested hollow cones of emission, which, along with a central core emission region, make up the complete pulsar emission beam. The actual profile observed for a given pulsar depends on the cut that the observer's line of sight makes through this emission beam. From the above work, Rankin also concludes that core radiation originates from very close to the neutron star surface, whereas the conal radiation comes from regions higher up in the magnetosphere. The outer cone is postulated to originate higher up in the magnetosphere than the inner cone but along the same set of field lines. Recent work by Gil et al. (2002), which compares frequency dependence of pulsar radiation features for average profiles with those for single pulses, comes up with evidence in support of such a conal beam model. A somewhat different model of the pulsar emission beam is described by Lyne & Manchester (1988), who propose that the emission within the beam is patchy; i.e., the distribution of component locations within the beam is random rather than organized in one or more hollow cones.

One of the problems in resolving this conflict is related to a correct determination of the total number of emission components for a pulsar and the significance of their arrangement within the pulse window. In a recent paper (Gangadhara & Gupta, 2001, hereafter Paper I), we have addressed these issues with the help of a novel method of studying the emission geometry of pulsars. Using the sensitive "window-thresholding" technique ("W-T" technique hereafter) on single-pulse data for a given pulsar, we first identify all possible conal emission components in the profile that can be detected, given the sensitivity of the data, and determine accurate locations in pulse longitude for these. From this we determine the total number and arrangement of emission cones in the observed profile. Then, from detection of retardation and aberration effects in the locations of the conal components, we estimate the emission height for each cone. Coupling this with a dipolar field geometry and the available information about the relative orientations of the spin and rotation axes of the pulsar and the line of sight, we are able to identify the field lines from which each cone originates, thereby giving a complete solution for the emission geometry for each cone. Using this technique on single-pulse data for PSR B0329+54 at two different radio frequencies, we showed in Paper I that there are as many as nine identifiable components in this pulsar,

[1] Permanent address: NCRA (TIFR), Pune University Campus, Pune 411007, India.

arranged in the form of four concentric rings around the central core component. The emission heights for the cones were found to increase systematically from inner to outer cones for a given frequency, ranging from ~160 to ~1150 km. Also, for a given cone, the height was found to reduce with increasing frequency, providing direct proof of the commonly accepted "radius–to–frequency-mapping" paradigm.

In this paper we extend our study of emission geometry to another six pulsars. Section 2 describes the observations and data analysis steps. In § 3 we present our results, where we are able to solve for the emission geometry for five of the pulsars studied and have tentative results for the sixth. In § 4 we discuss the implications of our findings for the current understanding of pulsar emission physics.

2. OBSERVATIONS AND DATA ANALYSIS

For our study of emission geometry, we selected a set of pulsars with clearly defined properties that make it easy to apply the techniques used for PSR B0329+54 in Paper I. These included the following criteria: (1) the presence of multiple emission components (or indications thereof) in the existing profiles, (2) the presence of a reasonably well identified core component at our frequency of observation, which was the 325 MHz band of the Giant Metrewave Radio Telescope (GMRT), and (3) mean flux strong enough that reasonable signal-to-noise ratio (S/N) could be expected for single-pulse observations with the incoherent array mode of the GMRT. The first two constraints above confine the selected pulsars to the category of "triple" or "multiple" pulsars as defined by Rankin (1993) or, equivalently, to the category of "cone with core" pulsars, as defined by Lyne & Manchester (1988). Of the possible candidates, we avoided pulsars with very wide profiles (e.g., PSR B0826−34, PSR B1541+09), as it is not easy to unambiguously identify discrete emission components in these profiles because of the extended emission over a large fraction of the pulse period. The final list of pulsars selected for our study is given in Table 1, along with relevant details. Here α and β refer to the standard definitions of the angle between the rotation and magnetic axes and the impact angle of the line of sight with respect to the magnetic axis, respectively. The values for these angles are taken from Rankin (1993). These are not very different from the corresponding values given by Lyne & Manchester (1988)—the typical difference for α is ~a few degrees and that for β is less than ~0°.5–1°.0.

The observations were carried out at the GMRT, in the 325 MHz band, using the incoherent array mode (see Gupta et al. 2000 for more details about the pulsar modes of operation of the GMRT). The data were obtained by incoherent addition of the dual polarization signals from 12 antennas. The bandwidth used was 16 MHz, divided into 256 spectral channels by the digital back ends. The raw data were integrated to a time resolution of 0.516 ms before being recorded for off-line analysis, where the data were dedispersed and gated to obtain the single-pulse sequence for each pulsar. During this analysis, care was taken to check and flag the data for radio-frequency interference signals. For a majority of the pulsars, the center frequency of the observations was 318 MHz; for one case it was 328 MHz, and it was 333 MHz for another (see Table 1).

All of the 318 MHz observations were carried out on 2000 December 10–11. For most cases, the total number of pulses was obtained from a single observing run. For some pulsars (e.g., PSR B2045−16), data from different observing sessions (on different days) were combined (after proper alignment) to obtain the final single-pulse sequence with enough pulses for subsequent analysis. The total number of pulses for each pulsar is given in the seventh column of Table 1.

The average profile obtained for each pulsar is shown in Figure 1. The time resolution here is the basic sample time interval of 0.516 ms, except for the case of PSR B2111+46, where the data have been integrated by a factor of 4, to a sample interval of 2.064 ms. The S/N obtained for the peak of the average profiles is quite good—in the range 200–600—resulting in single-pulse peak S/Ns of the order 5–10 and better, which are needed for using the W-T technique effectively. All the pulsars show multiple-component profiles, with at least three or more components easily visible. The classification of each pulsar, according to the scheme proposed by Rankin (1993), is given in the sixth column of Table 1, where the triple (T) pulsars have three known components and the multiple (M) pulsars have five known components. From published results related to (1) frequency evolution of the profile components and (2) polarization properties of average profiles (e.g., Rankin 1993; Lyne & Manchester 1988 and references therein), it is clear for most of these pulsars that the central component is the core component. Further, in almost all cases, it is apparent from Figure 1 that the conal components are located asymmetrically with respect to the core component, with the tendency for each trailing conal component to be closer to the core than its leading counterpart. This is consistent with the expectations of retardation and aberration effects due to the finite emission height of the conal beams (e.g., Paper I).

To carry out a detailed modeling of the geometry of the emission cones for each pulsar, we need to identify all

TABLE 1
PROPERTIES OF THE PULSARS USED FOR EMISSION GEOMETRY STUDIES

Pulsar	Frequency (MHz)	Period (s)	α (deg)	β (deg)	Profile Class	Number of Single Pulses	Number of New Components
PSR B0450−18	318	0.5489	24.0	4.0	T	2405	?
PSR B1237+25	318	1.3824	53.0	0.0	M	1915	2
PSR B1821+05	318	0.7529	32.0	1.7	T	1435	4
PSR B1857−26	318	0.6122	25.0	2.2	M	2150	2
PSR B2045−16	328	1.9617	36.0	1.1	T	1680	3
PSR B2111+46	333	1.0147	9.0	1.4	T	2900	4

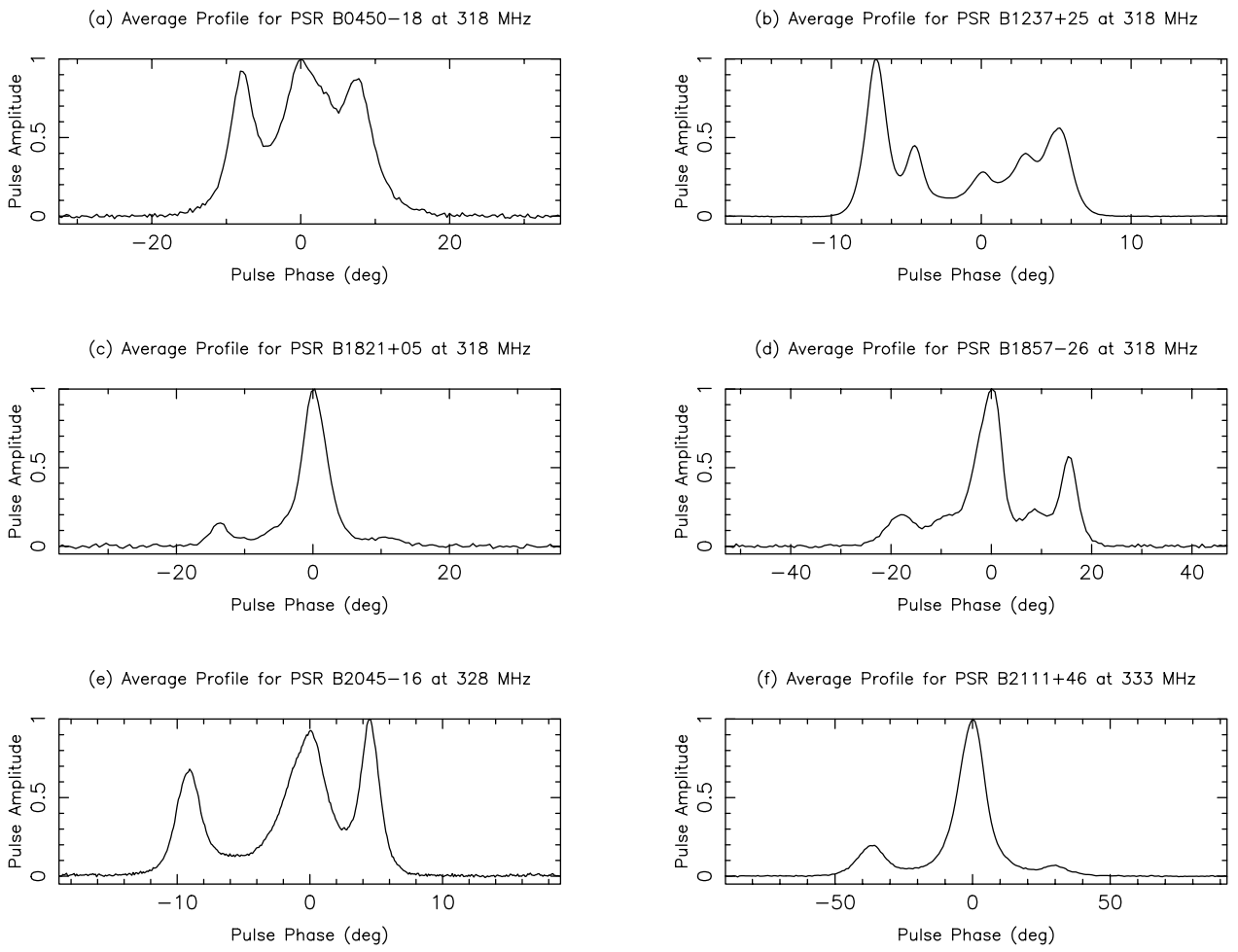

FIG. 1.—Average pulse profiles for the six pulsars. The time resolution is 0.516 ms for all except PSR B2111+46, for which it is 2.064 ms.

possible emission components in the profiles that can be determined within the S/N limitations of our data. For this we have used the W-T technique described by us in Paper I, where we employed this technique to identify as many as nine emission components in PSR B0329+54. In this technique, we set a window in a desired pulse longitude range and employ an intensity threshold to select the single pulses that go to make an average profile, which we refer to as a "W-T profile." We consider all those pulses that have emissions above the threshold within the window. As a result of this averaging of selected pulses, emission components within the window improve in S/N compared to other parts of the profile and are thus more easily detected in the W-T profile. As described in Paper I, we use a few different checks to ensure that the detected components are genuine. Usually, the window size and location are varied by a few bins while checking that the component shows up at the same location (this is not always possible to do for components that are located in close proximity to known, strong components). In addition, the selection threshold is varied over a reasonable range to check the persistence of the component and to minimize picking up contributions from random noise. These checks are robust enough to avoid detection of spurious components by chance accumulations in the selected window. This is supported by the fact that the W-T technique does *not* detect any new components when applied to off-pulse regions of the profile.

Using the W-T technique, we have been able to detect new emission components in most of the pulsars studied here, as well as get accurate estimates for the locations of the existing components. The total number of *new* components detected for each pulsar is given in the last column of Table 1. Some typical examples of detection of components (new as well as known ones) are illustrated in the sample of W-T profiles shown in Figure 2. Here Figures 2*a* and 2*e* show examples of clear and easy detections (usually of already known components); Figures 2*b*, 2*d*, and 2*g* illustrate detection of new, weak components, and Figures 2*c*, 2*f*, and 2*i* are cases of detections of new components located in close proximity to known, strong components. In some cases we were able to increase the confidence of our detections by integrating the data to a larger time constant (2–4 times the original sampling rate) and repeating the W-T analysis, albeit with a loss in resolution of the location of the component peak. This was particularly useful in cases where the original pulse profile is relatively broad and well sampled (e.g., PSR B2111+46) and the S/N is marginal for the weaker emission components.

In some cases, we detect likely candidates for new emission components but cannot confirm them with enough confidence from our data set. This is due to limitations of (1) inadequate S/N, (2) not enough pulses for the weak components to show up reliably often enough, or (3) very close proximity of the suspected component to a known

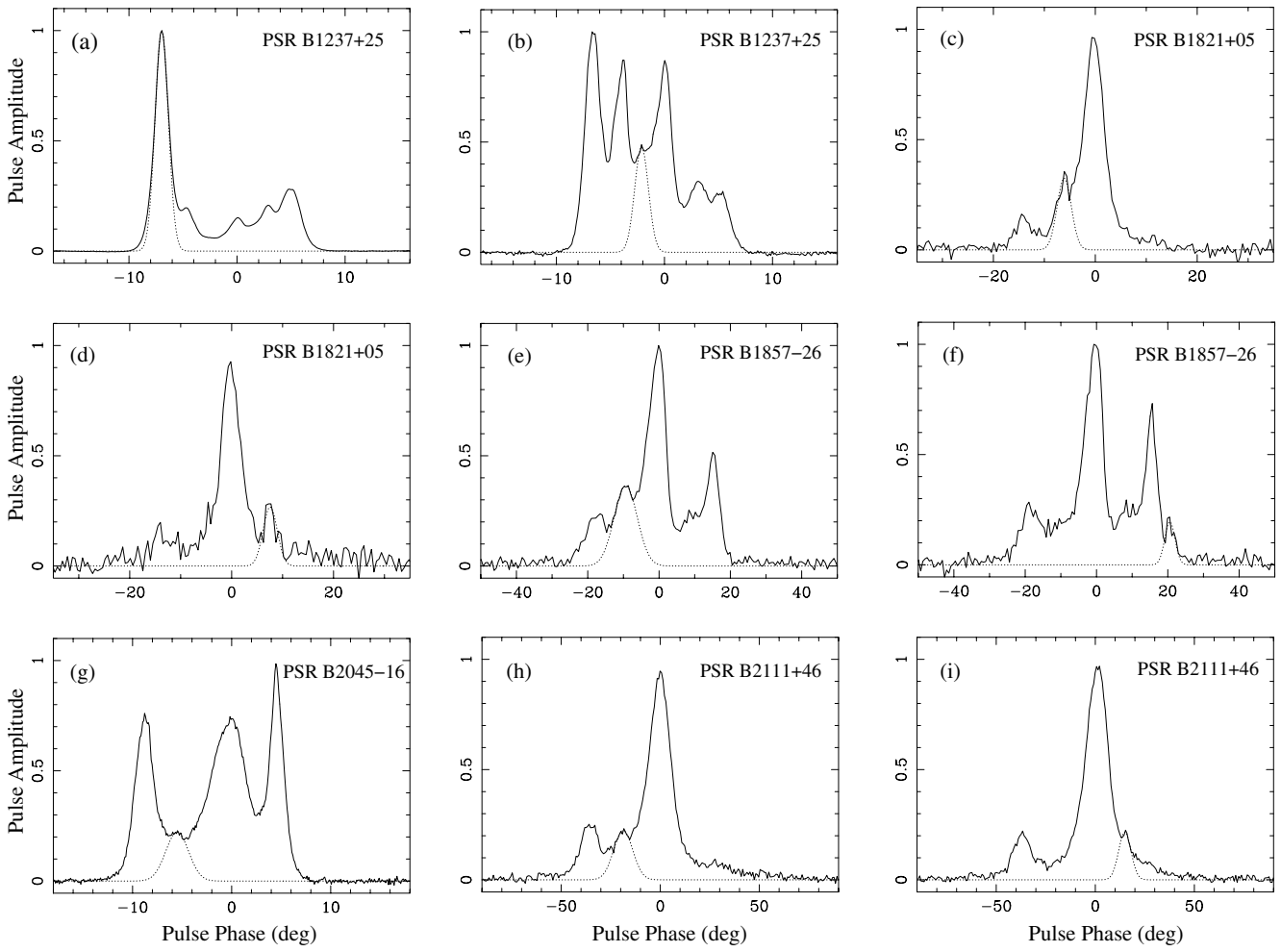

FIG. 2.—Examples of detection of emission components. The solid curves are the W-T profiles, and the dotted curves show the best-fit Gaussian model for the detected component.

component, especially when the latter is a strong component. In such cases, we label the component detection as "tentative." We mention this specifically for each pulsar when we discuss the individual results.

To determine accurate locations in pulse longitude for each component of a pulsar, we take the corresponding W-T profile and fit a Gaussian curve to the selected component. The noise contribution to each data point is estimated from the off-pulse noise rms of the W-T profile. The peak of the best-fit Gaussian is taken as the best estimate of the location of the component, and the 1 σ error estimate on this peak is used to derive the error in the location of the component. For the sample detections shown in Figure 2, we also show the best-fit Gaussian to the component detected within the W-T window. For most cases, we get quite good fits, with values for the reduced $\chi^2 \sim 1.0$. The error estimates are generally found to be proportional to the S/N of the fitted component, which is as expected.

From our determination of the total number of the emission components, we resolve the emission geometry for each pulsar as consisting of a central core component and one or more cones of emission around it. From our best estimates of the locations of these components, we then solve for the emission heights of the cones, as well as for the transverse location of the emitting field lines on the polar cap, using the technique described in Paper I. The polar cap location of the field lines is quantified by the ratio of the distance to the "foot" of the field line (from the magnetic pole) to the distance to the "foot" of the last open field line in the magnetosphere—the parameter s_L^i of Paper I (in this description, the foot of the field line is the point where the field line intersects the neutron star surface).

3. RESULTS

The results from our analysis of the six pulsars are summarized in Tables 2–7. The table for each pulsar gives, for every emission cone that we detect (including the known ones), the following information: ϕ_l^i and ϕ_t^i, the location (with respect to location of the core component) of the leading and trailing emission components that constitute the cone (second and third columns); η^i, the inferred retardation plus aberration angle (fourth column); Γ^i, the inferred half angle of the conal beam (fifth column); $r_{\rm em}^i$, the computed emission height for the cone (sixth column); and s_L^i, the polar cap location of the associated field lines (seventh column). The emission heights of the cones are given in kilometers, as well as the fraction of the light-cylinder radius ($r_{\rm LC}$) in the sixth column. The errors for the derived quantities (fourth through seventh columns) are determined from

TABLE 2
EMISSION GEOMETRY RESULTS FOR PSR B0450−18

Cone Number	ϕ_l^i (deg)	ϕ_t^i (deg)	η^i (deg)	Γ^i (deg)	$r_{\rm em}^i$ (km) (% $r_{\rm LC}$)	s_L^i
1.....	-8.79 ± 0.10	6.76 ± 0.11	-1.01 ± 0.11	5.25 ± 0.02	310 ± 30 (1.2%)	0.56 ± 0.03

appropriate propagation of the errors on the estimates of the emission component locations (including that for the core component) and do not include any effects of possible errors in the values of α and β.

We first discuss the results for individual pulsars and present a general summary of the results at the end of this section.

3.1. *PSR B0450−18*

This pulsar shows a three-component profile for frequencies below about 1 GHz and is interpreted as a typical triple (core and one conal pair) pulsar (e.g., Rankin 1993). However, this classification is not completely unambiguous. Although the frequency evolution of the components (e.g., Gould 1994) appears to indicate that the central component is a core, the polarization characteristics do not show clear, unambiguous evidence of core radiation for this component. At our frequency, the profile shows a fairly wide emission region around the central peak, especially on the trailing side (Fig. 1). The W-T analysis readily localizes the leading and trailing components in the profile. However, in the central 10°–15° of pulse longitude we get unclear and conflicting results. The W-T analysis shows evidence for multiple emission peaks in this region (e.g., at $-4\overset{\circ}{.}1$ and 3°), but these are generally not found to be stable against variations of window widths and thresholds. Hence, it is difficult to unambiguously identify distinct emission components in the central region, including a clear identification of the reference core component. It is possible that what we are seeing in this region is a somewhat tangential cut through the edge of an inner emission cone and that the core, if present at all, is a weak component in this region. This would be consistent with the fact that this pulsar has a relatively large value of the impact parameter β—it is the largest amongst all the pulsars studied here (Table 1). The entry in the eighth column of Table 1 for this pulsar reflects our uncertainty in the identification of new emission components.

Using a tentative identification of the core as the peak produced by setting a wide window in the central region, we get the locations of the main leading and trailing emission components with respect to the core as $-8\overset{\circ}{.}79$ and $+6\overset{\circ}{.}76$, respectively. In addition, there is some evidence from our analysis for the presence of weak components in the leading and trailing wings of the profile, but these cannot be confirmed with the quality of our data. Solving for a single emission cone for this pulsar, the emission height and polar cap location are obtained as 310 km (1.2% of $r_{\rm LC}$) and 0.56, respectively (see Table 2). We note that the results for this pulsar should be treated with caution, as the emission geometry is probably more complicated than what we present.

3.2. *PSR B1237+25*

The typical average profile for this well-studied pulsar clearly shows five emission components with the central one known to be the core component. The centers of both cones are clearly offset to earlier longitudes than the core, as would be expected because of retardation and aberration. Our analysis reveals the presence of two more emission components, located between the core and the inner conal ring. Of these two, the component on the leading side (at $-2\overset{\circ}{.}12$) is seen relatively easily in our analysis (Fig. 2*b*), whereas the one on the trailing side (at $+1\overset{\circ}{.}56$) is somewhat harder to detect. This is because it is located in the relatively narrower region between the core and the trailing component of the inner cone. We therefore interpret this pulsar as having three emission cones around the core component, with each cone clearly showing retardation and aberration effects. Solving for the locations of the emission cones at 318 MHz gives heights of 180, 460, and 600 km (0.3%, 0.7%, and 0.9% of $r_{\rm LC}$, respectively) and transverse locations on the polar cap of 0.33, 0.41, and 0.59 (see Table 3).

3.3. *PSR B1821+05*

The average profile for this pulsar shows a core-dominated triple-component emission beam at 318 MHz (Fig. 1). The conal components, located at $-13\overset{\circ}{.}75$ and $+10\overset{\circ}{.}94$, clearly exhibit retardation-aberration effects. Even though the S/N is not very good, there are indications of extra emission components between the core and the known conal components. With some difficulty, our analysis picks up a component at $-6\overset{\circ}{.}07$ from the core and one at $+8\overset{\circ}{.}2$ on the trailing side (Figs. 2*c* and 2*d*). In addition, we have marginal detections of two more conal components, at $-10\overset{\circ}{.}25$ and $+4\overset{\circ}{.}61$. These last two are detected with fairly low thresholds in the W-T technique and are, at best, tentative detections, requiring confirmation with higher sensitivity observations. Analysis of the data after further integration by a factor of 2 was used to confirm the presence of these components.

TABLE 3
EMISSION GEOMETRY RESULTS FOR PSR B1237+25

Cone Number	ϕ_l^i (deg)	ϕ_t^i (deg)	η^i (deg)	Γ^i (deg)	$r_{\rm em}^i$ (km) (% $r_{\rm LC}$)	s_L^i
1.....	-2.12 ± 0.07	1.56 ± 0.09	-0.28 ± 0.07	1.47 ± 0.05	180 ± 40 (0.3%)	0.33 ± 0.04
2.....	-4.41 ± 0.03	2.98 ± 0.06	-0.72 ± 0.05	2.95 ± 0.03	460 ± 30 (0.7%)	0.41 ± 0.02
3.....	-6.97 ± 0.02	5.11 ± 0.02	-0.93 ± 0.04	4.82 ± 0.01	600 ± 30 (0.9%)	0.59 ± 0.01

TABLE 4
EMISSION GEOMETRY RESULTS FOR PSR B1821+05

Cone Number	ϕ_l^i (deg)	ϕ_t^i (deg)	η^i (deg)	Γ^i (deg)	$r_{\rm em}^i$ (km) (% $r_{\rm LC}$)	s_L^i
1.....	-6.07 ± 0.47	4.61 ± 0.30	-0.73 ± 0.31	3.36 ± 0.13	290 ± 120 (0.8%)	0.43 ± 0.09
2.....	-10.25 ± 0.30	8.20 ± 0.43	-1.03 ± 0.29	5.28 ± 0.13	410 ± 120 (1.2%)	0.57 ± 0.08
3.....	-13.75 ± 0.39	10.94 ± 0.27	-1.41 ± 0.27	6.90 ± 0.12	570 ± 110 (1.6%)	0.64 ± 0.06

Our final result for this pulsar is a detection of three cones for which the emission heights at 318 MHz are obtained as 290, 410, and 570 km (0.8%, 1.2%, and 1.6% of $r_{\rm LC}$, respectively), and polar cap locations are obtained as 0.43, 0.57, and 0.63, respectively (see Table 4).

3.4. *PSR B1857−26*

This is a well-known multiple-component (M-type) pulsar, where the typical profile at meter wavelengths readily shows four components and has clear indications of a fifth component located close to the leading edge of the central, core component (see Fig. 2*e* for our detection of this component). Our analysis easily gives the locations for these five known components. In addition, we see evidence for two more outer components, located near the leading and trailing edges of the profile, at $-23\overset{\circ}{.}73$ and $+19\overset{\circ}{.}95$ with respect to the core (see Fig. 2*f* for one of these). We label these two as tentative detections, as the threshold and number of contributing pulses are rather small (although the analysis of data integrated by a factor of 2 supports these detections). Further, there are hints of emission components in between the known conal components, but these cannot be confirmed with the quality of our data.

We thus have five confirmed components (along with two tentative ones) for this pulsar, leading to an interpretation of core and two emission cones (and a tentative third outer cone). The emission heights (at 318 MHz) for these three cones are found to be 220, 480, and 690 km (0.8%, 1.7%, and 2.4% of $r_{\rm LC}$) and polar cap locations of 0.61, 0.69, and 0.74 (Table 5).

3.5. *PSR B2045−16*

This well-known pulsar shows a three-component profile where the central core component is clearly asymmetrically located with respect to the center of the conal ring. This is an indication of significant aberration and retardation effects for the emission cone. On using the W-T technique, we are able to detect three more emission components, located in the "saddle" regions between the core and the known conal components, at longitudes of $-7\overset{\circ}{.}2$, $-5\overset{\circ}{.}5$, and $+3\overset{\circ}{.}06$ with respect to the core (see Fig. 2*g* for an example of one of these). This gives a total of five conal components, leaving us with the somewhat difficult situation of a probable undetected conal component, which needs to be located in the narrow valley between the core and the already known trailing conal component. There are some indications of an emission component at $+4\overset{\circ}{.}0$, but we cannot determine this unambiguously from our analysis, as it is too close to the known component at $+4\overset{\circ}{.}59$. Lacking this, we have the problem of deciding which of the three new conal components is the odd one out. If we take the components at $-5\overset{\circ}{.}5$ and $+3\overset{\circ}{.}06$ as forming the second conal ring, the solutions for the two rings are emission heights at 1240 and 2230 km (1.3% and 2.4% of $r_{\rm LC}$) and polar cap locations of 0.28 and 0.32—this is the solution listed in Table 6. Alternatively, taking the components at $-7\overset{\circ}{.}2$ and $+3\overset{\circ}{.}06$ as forming the second conal ring changes the emission height estimate for this cone from 1240 to 2090 km, and the polar cap location shifts from 0.28 to 0.22. We believe the first option is more likely to be the real situation.

3.6. *PSR B2111+46*

This pulsar shows a very wide but clearly triple profile with a dominant core component at meter wavelengths (Fig. 1). The location of the conal components is clearly asymmetric with respect to the core, showing retardation-aberration effects. For this pulsar two data sets, one taken at 318 MHz in 2000 December and another taken at 333 MHz in 2002 February were available. Since the data from February 2002 had better S/N and more number of pulses, all the results presented here are from the analysis of this data set. Analysis of the 2000 December data produced results that are similar to those reported here and well within the errors of the measurements.

Since the profile is very wide, the data were averaged to 4 times the original time resolution of 0.516 ms to improve the S/N for the W-T analysis. Besides confirming the location of the main components, our W-T analysis picks up two additional conal components, located at $-18\overset{\circ}{.}71$ and $+14\overset{\circ}{.}91$ with respect to the core (see Figs. 2*h* and 2*i*). In addition, there are hints of another pair of components located at the leading and trailing edges of the profile (at approximately $-48\overset{\circ}{.}3$ and $+38\overset{\circ}{.}7$ with respect to the core), but we are unable to confirm them clearly. Hence, for this pulsar we confine ourselves to two cones of emission around the central core component. The estimates for the emission

TABLE 5
EMISSION GEOMETRY RESULTS FOR PSR B1857−26

Cone Number	ϕ_l^i (deg)	ϕ_t^i (deg)	η^i (deg)	Γ^i (deg)	$r_{\rm em}^i$ (km) (% $r_{\rm LC}$)	s_L^i
1.....	-9.78 ± 0.25	8.51 ± 0.25	-0.64 ± 0.20	4.58 ± 0.07	220 ± 70 (0.8%)	0.61 ± 0.10
2.....	-18.06 ± 0.11	15.30 ± 0.07	-1.38 ± 0.11	7.64 ± 0.03	480 ± 40 (1.7%)	0.69 ± 0.03
3.....	-23.73 ± 0.46	19.95 ± 0.34	-1.96 ± 0.30	9.77 ± 0.12	690 ± 100 (2.4%)	0.74 ± 0.06

TABLE 6
EMISSION GEOMETRY RESULTS FOR PSR B2045−16

Cone Number	ϕ_l^i (deg)	ϕ_t^i (deg)	η^i (deg)	Γ^i (deg)	$r_{\rm em}^i$ (km) (% $r_{\rm LC}$)	s_L^i
1.....	-5.50 ± 0.28	3.06 ± 0.13	-1.22 ± 0.16	2.78 ± 0.08	1240 ± 160 (1.3%)	0.28 ± 0.02
2.....	-8.97 ± 0.04	4.59 ± 0.03	-2.19 ± 0.05	4.18 ± 0.01	2230 ± 50 (2.4%)	0.32 ± 0.004

heights at 333 MHz are 1360 and 2080 km (2.8% and 4.3% of $r_{\rm LC}$), while the values for the polar cap locations are 0.22 and 0.31 (see Table 7).

3.7. *Summary of Results*

Our main results can be summarized as follows:

1. All six pulsars show clear signatures of an asymmetry of the cones with respect to the core radiation in that the centers of the cones occur at earlier pulse longitudes with respect to the location of the core. For a given pulsar, the magnitude of the effect increases from inner to outer cones.
2. Interpreting the shift of the cone centers as the effect of retardation and aberration on the emitted conal beam leads to reasonable values for the emission heights. These range from about 200 to 2200 km over all six pulsars. In terms of the light-cylinder distance, this range is from 0.3% to 4.3% of $r_{\rm LC}$. For a given pulsar, the heights are found to increase systematically from the inner to the outer cones (although in some cases the sizes of the error bars prevent this from being made a firm conclusion).
3. Combining the emission height estimates with a dipole field line geometry results in estimates of the transverse polar cap locations of the foot of the field lines that each cone is radiated from. These are found to vary from about 0.22 to 0.74 of the radial distance to the last open field line from the magnetic axis. Furthermore, this value is found to increase systematically from inner to outer cones for a given pulsar (although again, for some cases, the sizes of the errors reduce the significance of this conclusion).

4. DISCUSSION

There are several interesting aspects of pulsar emission geometry that can be addressed by our study. First, it should be clear from this work (and Paper I) that it is not sufficient to study only the average profiles to understand the emission geometry. We have shown that a careful analysis of good-quality single-pulse data can provide valuable extra information about the emission geometry. It would be almost impossible to detect some of the emission components that we have detected by means of techniques such as fitting multiple Gaussians to the average profile. Here the window-thresholding method used by us comes in as a handy tool to find components that are weak and/or emit intermittently or those which are located close to other strong components. Using this, we find that most triple- and multiple-component pulsars can be shown to have five or seven components. It is then likely that most pulsars, when observed with sufficient quality data, are going to show multiple emission cones around the central core component.

Further, a careful identification of the emission components appears, almost invariably, to support the picture of a core beam plus multiple, concentric conal beams of emission in that the conal components turn out to be arranged in equal numbers on either side of the core. What is even more interesting is that in all cases, there is an asymmetry in the location of the core with respect to the centers of the cones, and that too always in the same sense of having the cone centers advanced with respect to the core component location. Although we have presented the detailed analysis for only a handful of pulsars, this trend is easily visible in a vast majority of pulsars that have clearly defined core and conal emission components. A check of the data from different sources in the literature (e.g., Gould 1994; Hankins & Rickett 1986; Weisberg et al. 1999; the European Pulsar Network [EPN] database) reveals several clear cases: PSR B0105+68, PSR B1700−32, PSR B1737+13, PSR B1826−17, PSR B1916+14, PSR B1946+35, PSR B2002+31, and PSR B2003−08 (detailed studies of several such pulsars have been initiated and will be reported on shortly). Thus it would seem that this is a fairly universal trend among pulsars that show clear core and conal emission components, and our interpretation of this as being due to retardation-aberration effects in the magnetosphere, is a reasonable one.

The emission heights that we obtain for the different pulsars have very plausible values. For PSR B0450−18, PSR B1237+35, PSR B1821+05, and PSR B1857−26, we obtain emission heights in the range of 200–700 km, while for PSR B2045−16 and PSR B2111+46, the values range from 1200 to 2200 km. Typical estimates of emission heights reported in literature are a few hundred kilometers for most pulsars (e.g., Rankin 1993; Kijak & Gil 1998). Rankin (1993) estimates the emission heights for the cones from the measured half-power widths of the conal component pairs and makes the assumption that the cones are radiated from near the last open field lines of the polar cap. This yields 1 GHz height estimates of about 130 and 220 km for the two cones.

TABLE 7
EMISSION GEOMETRY RESULTS FOR PSR B2111+46

Cone Number	ϕ_l^i (deg)	ϕ_t^i (deg)	η^i (deg)	Γ^i (deg)	$r_{\rm em}^i$ (km) (% $r_{\rm LC}$)	s_L^i
1.....	-18.71 ± 0.72	14.91 ± 0.53	-1.90 ± 0.45	3.14 ± 0.07	1360 ± 320 (2.8%)	0.22 ± 0.03
2.....	-35.69 ± 0.11	29.87 ± 0.16	-2.91 ± 0.11	5.61 ± 0.02	2080 ± 80 (4.3%)	0.31 ± 0.006

Our height estimates will naturally be larger than these, as we find that the emission is located on field lines that are well inside of the last open field line: a cone of the same angular width radiated from inner field lines has to come from a greater height in the magnetosphere. Specifically, for PSR B1237+25 and PSR B1857−26, Rankin (1993) gives estimates of emission heights for the cones at a range of frequencies. Comparing with the values at the nearby frequency of 270 MHz (Table 3 of Rankin 1993), we find that our estimates for the same cone at 318 MHz are more than twice as large. If, however, the estimates of Rankin (1993) are corrected for emitting field line with $s_L^i \sim 0.6$ (as postulated in Mitra & Rankin 2002), then the results are in better agreement with ours. Our emission height estimates are closer to those obtained by Kijak & Gil (1997, 1998), although still somewhat larger.

We note that the height estimates for PSR B2045−16 and PSR B2111+46 are somewhat unusually large. Correspondingly, these two pulsars also have rather small values for the polar cap locations of the radiating field lines, as compared to the lower emission height pulsars. The reason for these larger heights is not clear. As a fraction of the light-cylinder radius distance, however, all these heights are still quite small, being ∼5% of $r_{\rm LC}$ at the largest. This also means that effects of magnetic field sweepback (see Paper I) can safely be ignored for all these cases.

Strictly speaking, all our height estimates are heights of the cones *relative to that of the core radiation*, as the retardation-aberration of the cone centers is measured with the core component as reference. Since the core radiation is thought to originate very close to the neutron star surface (e.g., Rankin 1990, 1993), these are good estimates for the actual emission heights of the cones above the neutron star surface (the extra height of 10 km for the radius of the neutron star is much smaller than our typical error bars). However, if this assumption about the height of the core emission beam is not correct, then the height of the core emission has to be added to the height estimates we have reported for the cones—in this sense, our results can be taken as lower limits to the actual emission heights. The other effect of a finite core height will be to cause the inferred polar location of the cones to become somewhat smaller (see eq. [15] of Paper I), with the fractional change diminishing progressively from inner to outer cones. For example, an emission height of 100 km for the core radiation of PSR B1237+25 would cause the polar cap locations of the cones to reduce to 0.26, 0.37, and 0.55 from their present values of 0.33, 0.41, and 0.59. In any case, it is quite clear from our results that the core emission originates at heights that are substantially (∼hundreds of kilometers) less than that for the cones—otherwise we would not see any relative retardation-aberration effects between the core and cones.

Another interesting feature of the results is that they are quite self-consistent with radio emission originating within the open field line region of the magnetosphere in that we do not obtain results for polar cap locations that are greater than 1.0. This can happen in principle, as the emission height estimate is completely independent of the width of the cone, whereas both these parameters are relevant for the calculation of the polar cap location (see eqs. [9] and [15] of Paper I). Polar cap locations greater than 1.0 can result if the emission height estimates are less than the current results by factors of 4–16. In a sense then, this argues that our interpretation of component location asymmetries as being due to retardation-aberration effects is a sensible interpretation.

Perhaps the most interesting result from this work is that the different cones for a pulsar originate on different sets of field lines in the magnetosphere. Clearly, not all the conal radiation originate near the last open field line region. In fact, it appears that a significant fraction of the polar cap region may be active in the generation of the multiple conal beams. Furthermore, our results indicate that this activity is confined along distinct and concentric rings on the polar cap. Generally, it is thought (e.g., Ruderman & Sutherland 1975; Cheng & Ruderman 1980) that this activity may be produced by spark discharges in vacuum gaps formed immediately above the neutron star surface. For such a model, our results indicate that the sparks are confined to concentric rings on the polar cap. We note that there are recent reports of inference of such patterns of circulating sparks for pulsars with conal-single geometries showing drifting subpulses (e.g., Deshpande & Rankin 1999). Our results tend to support a similar conclusion for multiple-component pulsars with more central traverses of the observing line of sight. For our pulsars, we can actually constrain the radii of these rings via the s_L^i parameter. For a 10 km radius neutron star with a period of P s, the radial size of the polar cap is just $145P^{-0.5}$ m. For three concentric conal rings anchored to field lines at $s_L^i = 0.33$, 0.41, and 0.59 (as in PSR B1237+25), this translates to ring radii of 41, 51, and 73 m. Similar numbers (∼a few to several tens of meters) are obtained for other pulsars also. It is indeed remarkable that we can infer the presence of features of this size on the polar cap.

Gil & Sendyk (2000) have recently proposed a model for pulsar radiation that invokes concentric rings of sparks to explain the observed properties of pulsar radiation. In their theory, the separation between concentric rings of sparks, very close to the neutron star surface, is of the order of h, the height of the vacuum gap. They estimate the value of h to be of the order of 10 m for pulsars with period ∼1 s, which is quite similar to the typical separation of rings that we infer. For example, for PSR B1237+25, the separation between first and second rings is 10 m and that between the second and third is 22 m. For PSR B1821+05, these numbers are 23 and 12 m, respectively; for PSR B1857−26, they are 15 and 9 m. Thus our results make interesting connections with some of the existing theoretical models and support the idea of concentric rings of sparks circulating on the polar cap as being the cause of the radio radiation.

Although the activity that is the ultimate source of the radio radiation that we observe may be occurring very close to the neutron star surface, the final radiation that we see appears to originate at significant heights in the magnetosphere. Further, we have shown that the inner cones are emitted at lower altitudes and outer cones at progressively higher altitudes. In addition, it is generally accepted that the same cone is emitted at higher heights at lower frequencies. Clearly, all this is pointing to the requirement of the appropriate combination of parameters at specific points in the magnetosphere for the plasma disturbance to produce a beam of radiation that can be seen along our line of sight through the magnetosphere. This could be a combination of physical and geometrical parameters that contrive to give the right conditions at specific points in the magnetosphere. The localization of the emitting regions achieved by the kind of work reported here and in Paper I should help in better

constraining the parameter space and thus help the theories trying to find the correct explanation for the generation of the radio waves.

5. CONCLUSIONS

Using the window-thresholding technique to analyze single-pulse data from observations in the 325 MHz band of the GMRT, we have conducted a detailed analysis of the emission geometry of six radio pulsars that have prominent, multiple-component profiles. We have been able to detect new emission components in almost all of the pulsars. In some cases, we report tentative detections of weak components that need further confirmation studies. It thus looks likely that many multiple component pulsars may have at least five to seven components. The total number and location of the emission components we detect clearly supports a picture of multiple conal beams around a central core beam for these pulsars (and are a pointer to the possibility that most pulsars may have such an emission-beam structure).

Further, for all cases of conal emission, we find that the cone center is offset to earlier longitudes with respect to the location of the core, and this effect increases in magnitude from the innermost to the outermost cones for every pulsar. It appears this effect may be present in most pulsars that have clear core and conal emission geometries. We interpret this effect as being due to retardation and aberration of the conal emission beams in the magnetosphere of the pulsar. From this we are able to solve for the emission geometry and estimate the emission height for each cone and also the polar cap location of the field lines associated with the cone, following the technique developed in Gangadhara & Gupta (2001). We find emission height estimates in the range of 200–700 km for four pulsars, PSR B0450−18, PSR B1237+25, PSR B1821+05, and PSR B1857−26, and 1200–2200 km for two others, PSRs B2045−16 and B2111+46. In terms of the light-cylinder distance, the emission altitudes range from 0.3% to 4.3%. The estimates for the polar cap location of the radiating field lines come out to be in the range 0.22–0.74 times the distance to the last open field line from the magnetic axis. Further, for every pulsar with multiple cones, the emission altitude and the polar cap location are found to increase systematically from the innermost to the outermost cone.

Mapping the locations of the field lines associated with each cone onto the neutron surface gives concentric rings with radii of the order of a few to several tens of meters and spacings between adjacent rings of about 10–20 m. Our results thus tend to support a model of concentric rings of sparks produced in the vacuum gap region just above the neutron surface (e.g., Gil & Sendyk 2000).

The fairly precise localization of emission regions that we have reported should provide additional information for constraining the parameter space for theories and models of radio emission mechanisms.

We thank P. Ahmadi and the staff of the GMRT for help with the observations. The GMRT is run by the National Centre for Radio Astrophysics of the Tata Institute of Fundamental Research. We wish to thank the referee for useful suggestions that helped improve the quality of the results and J. Gil and T. Hankins for comments on the manuscript. In addition, Y. G. would like to acknowledge the support of the Arecibo Observatory of the NAIC for a sabbatical visit, during which the bulk of the work on this manuscript was done.

REFERENCES

Cheng, A. F., & Ruderman, M. A. 1980, ApJ, 235, 576
Deshpande, A. A., & Rankin, J. M. 1999, ApJ, 524, 1008
Gangadhara, R. T., & Gupta, Y. 2001, ApJ, 555, 31 (Paper I)
Gil, J. A., Gupta, Y., Gothoskar, P. B., & Kijak, J. 2002, ApJ, 565, 500
Gil, J. A., & Sendyk, M. 2000, ApJ, 541, 351
Gould, D. M. 1994, Ph.D. thesis, Univ. Manchester
Gupta, Y., Gothoskar, P. B., Joshi, B. C., Vivekanand, M., Swain, R., Sirothia, S., & Bhat, N. D. R. 2000, in IAU Colloq. 177, Pulsar Astronomy, ed. M. Kramer, N. Wex, & R. Wielebinski (ASP Conf. Ser. 105; San Francisco: ASP), 277
Hankins, T. H., & Rickett, B. J. 1986, ApJ, 311, 684
Kijak, J., & Gil, J. 1997, MNRAS, 288, 631
———. 1998, MNRAS, 299, 855
Lyne, A. G., & Manchester, R. N. 1988, MNRAS, 234, 477
Mitra, D., & Rankin, J. M. 2002, ApJ, 577, 322
Rankin, J. M. 1990, ApJ, 352, 247
———. 1993, ApJS, 85, 145
Ruderman, M. A., & Sutherland, P. G. 1975, ApJ, 196, 51
Weisberg, J. M., et al. 1999, ApJS, 121, 171